Invited Paper

Nondestructive evaluation of different material inclusions in glass fiber reinforced polymer composites by terahertz imaging

Jie Wang [1], Jin Zhang [1*], Tianying Chang [1, 2], and Hong-Liang Cui [1, 3]

[1] College of Instrumentation and Electrical Engineering, Jilin University, Changchun, Jilin, China 130061

[2] Institute of Automation, Qilu University of Technology (Shandong Academy of Sciences), Jinan, Shandong, China 250014

[3] Chongqing Institute of Green and Intelligent Technology, Chinese Academy of Sciences, Chongqing, China 400714

[*] Email: zhangjin0109@jlu.edu.cn

(Recived June 1, 2018)

Abstract: A glass fiber reinforced polymer (GFRP) solid panel hidden different material inclusions has been systematically detected via terahertz (THz) time domain spectroscopy (TDS) system. It is experimentally demonstrated that the defect detection effect of THz-TDS imaging technology is obviously different for several material inclusions. Under the transmission mode, the imaging effect of the inclusion is proportional to the attenuation degree difference of THz wave after penetrating the inclusion defect, whereas it depends on the refractive index difference between the inclusion and the epoxy GFRP solid panel under the reflection mode. Furthermore, X-ray computed tomography (CT) and ultrasonic imaging are also used to detect the GFRP solid panel. The detection results among THz-TDS, X-ray CT, and ultrasonic imaging with regard to fiber orientation, visualization of defect and inspection cost are comparatively analyzed to evaluate the correct location of THz-TDS technology in the traditional nondestructive evaluation (NDE) tools.

Keywords: Glass fiber reinforced polymer composites; Terahertz; X-ray; Ultrasound; Nondestructive evaluation.

doi: 10.11906/TST.091-101.2018.09.09

1. Introduction

Glass fiber reinforced polymer (GFRP) composites provide an alternative to metallic and

hazardous materials such as steel, aluminum, and asbestos. In the application of aerospace, transportation, building and other related industries, GFRP composites have a number of properties, such as high specific strength, light weight, strong corrosion resistance, excellent thermal, and acoustic insulation power [1]. The extensive application of GFRP composites requires the corresponding advanced nondestructive evaluation (NDE) technologies for failure detection in the process of manufacturing and service [2, 3].

Various NDE technologies capable of characterizing the defects in GFRP composites have been developed over the years. So far, the most well-known tools are X-ray computed tomography (CT) [4] and ultrasonic technologies [5]. However, they both have their own strengths and weaknesses. X-ray CT technology can provide clear images of the internal defect features. However, this method uses ionizing radiation, which is harmful to the human body [6, 7]. Ultrasonic technology has been widely used due to its simplicity of analysis and its advantages in localization of the defects. However, the lateral and axial spatial resolutions are limited and liquid coupling is required [8, 9]. Terahertz (THz) technology can provide non-ionizing and non-contact examination for non-conductive materials [10, 11]. Due to the remarkable properties of THz wave, THz time domain spectroscopy (TDS) technology was firstly introduced to NDE of fiber reinforced polymer composites in 2006, which has already become a new promising tool nowadays [12, 13].

A number of investigations using THz-TDS technology have been reported on defect detection of carbon fiber reinforced polymer (CFRP) composites [14-16], polymethacrylimide (PMI) foam [17-19], and GFRP composites [20-22]. However, other NDE techniques have not been employed simultaneously to perform a careful comparison with THz-TDS technology. In this paper, THz-TDS, X-ray CT and ultrasonic imaging are systematically carried out to detect GFRP composites with different material inclusions, and the results of these three NDE techniques are compared and discussed. The rest of the paper is organized as follows. Section 2 introduces the sample, the THz-TDS system, as well as the THz imaging algorithm. The THz-TDS, X-ray CT, and ultrasonic imaging measurement results are discussed and compared in Section 3. Finally, Section 4 is the summary and conclusion.

2. Sample and method

2.1 Preparation of the sample

An epoxy GFRP solid panel with different material inclusions is employed in this work. The panel consists of multilayer glass fiber cloths and epoxy resin adhesive, through a laminating process. The thickness of a single-ply glass fiber cloth is about 0.2 *mm*, and the laying direction of unidirectional glass fiber cloths is 0/90 deg. The overall size of the panel is 100 *mm* × 100 *mm* × 3 *mm*. Four square-shaped inclusions (20 *mm* × 20 *mm* × 0.1 *mm*) of different materials (Teflon, plastic, aluminum foil, and paraffin paper) are inserted into the panel at the same depth to simulate the defects. The insert depth of four inclusions is about 1.5 *mm* from the front surface of the panel. A three-dimensional rendering of the panel is shown in Fig. 1(a), and the colour of purple, green, red and blue corresponds to the inclusion of Teflon, plastic, aluminum foil, and paraffin paper, respectively. A schematic diagram of one square-shaped inclusion is shown in Fig. 1(b).

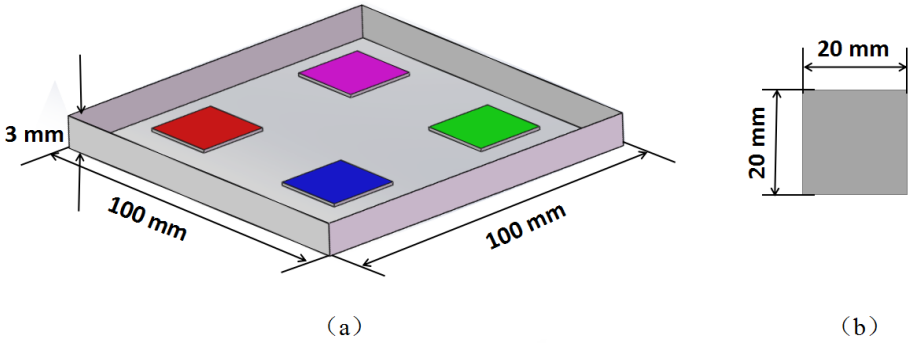

Fig. 1 Defect configuration of the epoxy GFRP solid panel: (a) three-dimensional rendering of the panel, and purple, green, red and blue correspond to Teflon, plastic, aluminum foil, and paraffin paper, respectively; (b) square-shaped inclusion.

2.2 THz experimental system

In this work, the FICO THz-TDS system from Zomega is employed, as shown schematically in Fig. 2. The femtosecond laser source generates a pulse with a central wavelength of 1520 *nm* and a duration of 250 *fs*. The time domain range is 0-100 *ps* with 0.05 *ps* resolution, and the effective spectral measure range is 0.1-2 *THz* with 11 *GHz* resolution. The minimum scanning step is 0.05 *mm* in both vertical and horizontal directions, and the maximum scanning range is 150 × 150 mm^2. The THz-TDS system has two modes of operation: transmission mode and reflection mode. During the sample testing procedure, the system is in a sealed chamber filled with dry air.

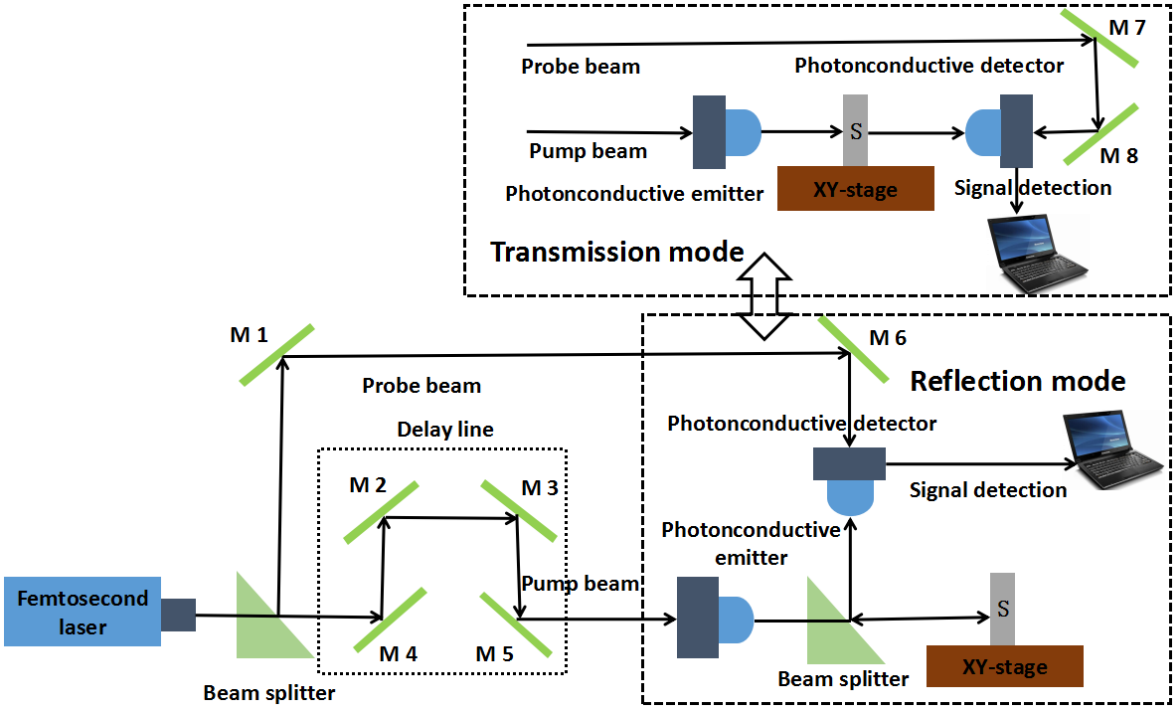

Fig. 2 Schematic diagram of THz-TDS system in both reflection and transmission modes (M1-M8: mirrors).

2.3 THz imaging algorithm

THz-TDS system scans the sample in both horizontal and vertical directions to acquire the time domain waveform for each spatial point of the sample. Two types of two-dimensional imaging can be established, commonly referred to as C-scan imaging and B-scan imaging. In the C-scan image, the abscissa and ordinate values represent the horizontal and vertical positions of the sample, respectively. THz C-scan imaging can be divided into time domain and frequency domain imaging. Time domain imaging can be established pixel by pixel based on the specific information from the time domain waveform, such as maximum peak, minimum peak, peak-to-peak, etc., whereas frequency domain imaging can be built up based on the specific information from the frequency domain waveform, such as amplitude, phase, refractive index, absorption coefficient, etc. at certain frequencies. For different samples, the information which can produce the best imaging effect must be individually determined, and generally varies from sample to sample. In the B-scan image, the abscissa values represent the horizontal or vertical positions of the sample, and the ordinate values represent the time delays (equivalent to depth of the sample).

3. Measurement results

3.1 THz measurement results

In this work, the scanning step size is set at 1 *mm*, and the scanning area is set at 100×100 mm^2 in both the transmission and reflection mode.

Figure 3 shows the THz C-scan imaging results of the sample. Figure 3(a) is the transmitted amplitude image at 0.3 *THz*. From Fig. 3(a), we can see that the detection effect of aluminum foil inclusion is the best, and plastic inclusion can hardly be detected. Figure 4 shows the transmitted waveforms extracted from the defection and non-defection regions on the sample, and the color of the waveforms corresponds to that of the rhombuses in Fig. 3(a), which mark the locations of the waveform acquisition. As can be seen from Fig. 4, the maximum peaks of the transmitted waveforms in non-defection, Teflon, plastic and paraffin paper region are 134.5, 126.2, 134.1 and 131.4, respectively, and that in the aluminum foil region is almost 0, which is because that THz wave can hardly penetrate the metallic materials. The difference of the maximum peaks between non-defection and aluminum foil region is the biggest, whereas that between non-defection and plastic region is the smallest, which verify the THz defection detection results in Fig. 3(a). Figure 3 (b) is the reflected amplitude image at 0.3 *THz*. From Fig. 3(b), we can only detect the aluminum foil inclusion. Figure 5 is the THz B-scan images of the sample, corresponding to the red dashed lines in Fig. 3(b), respectively. From Fig. 5, we can see that the four inclusions are nearly at the same depth, and the interface between the aluminum foil inclusion and the sample is the clearest. Figure 6 shows the whole reflected time domain waveforms extracted from the defection and non-defection regions on the sample. The color of the waveform corresponds to the rhombuses in Fig. 3 (b). From Fig. 6, we can determine that the reflected THz pulses from the system are at about 89 *ps*, the reflected THz pulses from the front surface of the sample are at about 23 *ps*, and the reflected THz pulses from the rear surface of the sample are at about 63 *ps*. During the 38-48 *ps*, the reflected THz pulses in different forms are from the inclusions, which are determined by the differences of the refractive index between the inclusions and the epoxy GFRP solid panel. When the difference of the refractive index is bigger, the amplitude of the reflected THz pulse from the inclusion is greater, and it is easier to detect the defect through the peak of the reflected THz pulse from the inclusion. The reflection from the aluminum foil inclusion is the biggest, and that from the plastic inclusion is the smallest, which is nearly submerged by the reflection of the glass fiber cloth. Figure 3(c) is the reflected time domain maximum peak imaging with time delay between 38-48 *ps*. As can be seen from Fig. 3(c), the four inclusions are almost detected, and the detection effect has been greatly improved. As can be

seen from Fig. 3(a) and 3(b), both in the transmitted and reflected imaging, the fiber orientations of the sample can be easily visualized.

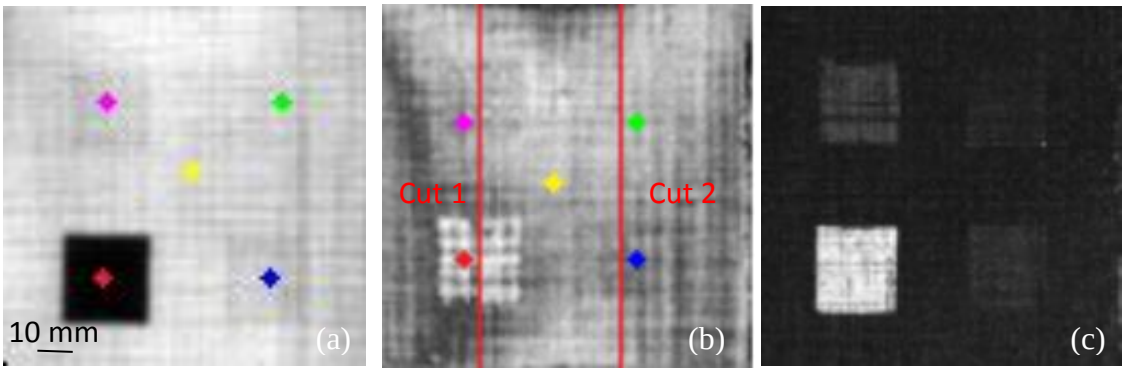

Fig. 3 THz C-scan imaging results of the sample: (a) transmitted, and (b) reflected amplitude image at 0.3 *THz*; (c) reflected time domain maximum peak imaging with time delay between 38-48 *ps*.

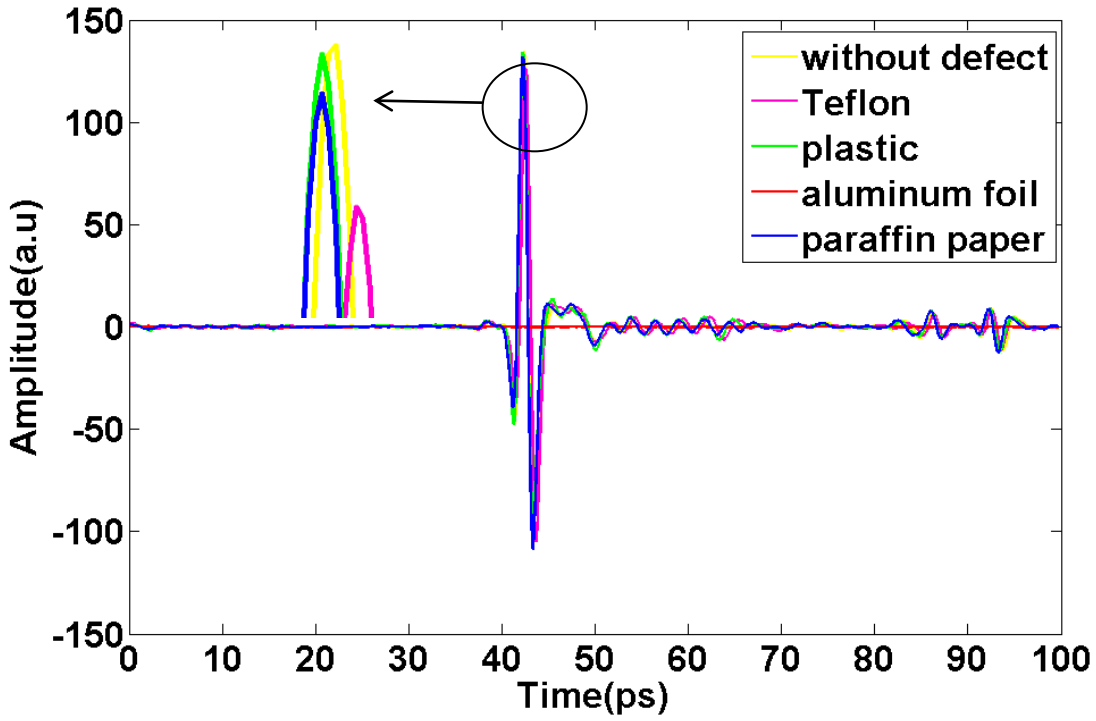

Fig. 4 Transmitted THz time domain waveforms measured from the sample, corresponding to the colored pixel dots in Fig. 3(a).

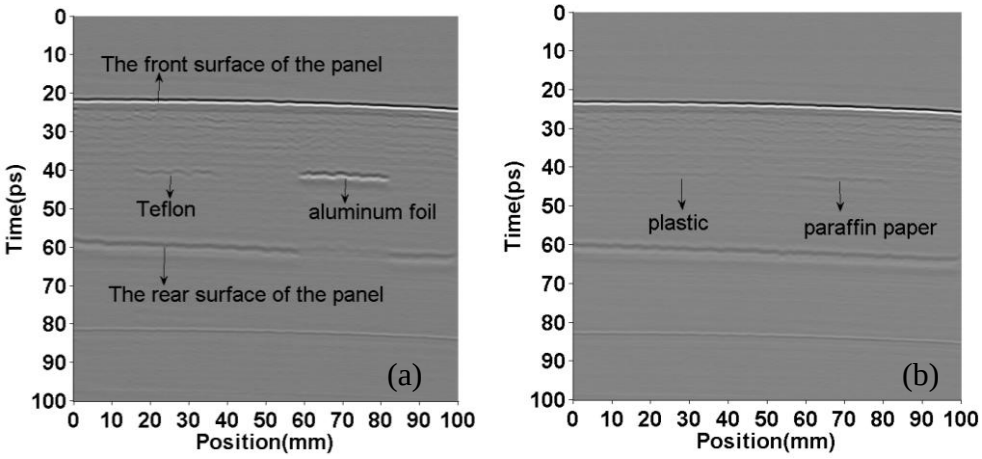

Fig. 5 Reflected THz B-scan imaging results of the sample: (a) Cut 1 and (b) Cut 2 column, corresponding to the vertical red dashed lines in Fig. 3(b), respectively.

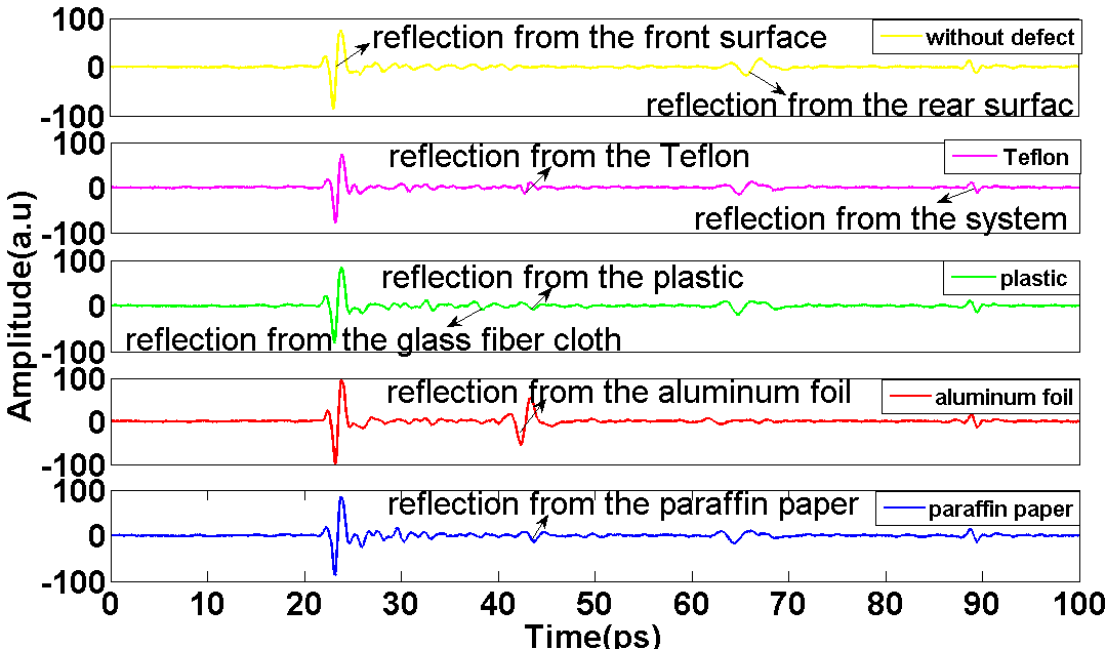

Fig. 6 Reflected THz time domain waveforms measured from the sample, corresponding to the colored pixel dots in Fig. 3(b).

3.2 Comparison with X-ray CT and ultrasonic measurement results

In order to verify THz imaging results, we used X-ray CT and ultrasonic imaging techniques to detect the sample. Figure 7(a) shows the CT image slice of the sample at depth of 1.45 *mm* in the axial direction. From Fig. 7(a), we can see that the aluminum foil inclusion can clearly be detected, the paraffin paper inclusion can barely be detected, and the Teflon inclusion and plastic

inclusion can hardly be detected. The inclusion detection effect depends on the density difference between the inclusion and the epoxy GFRP solid panel. Figure 7(b) shows the reflected ultrasonic imaging result of the sample. From Fig. 7(b), we can see that four inclusions of different materials can all be detected, but the shape detection of inclusions is not idea due to the poor resolution.

Comparison among THz-TDS, X-ray CT and ultrasonic imaging can be performed with respect to the following three aspects. (1) Fiber orientation: THz-TDS and X-ray CT imaging can observe the fiber orientations of the epoxy GFRP solid panel, whereas ultrasonic imaging fails. (2) Visualization of the defects: THz-TDS imaging has a better contrast ratio for the defect detection effect than X-ray CT imaging, and can provide better later resolution for the defect shape detection than ultrasonic imaging. (3) Inspection cost: X-ray CT imaging uses ionizing radiation, which is harmful to the human body. Ultrasonic imaging requires the liquid coupling, which may contaminate the sample. THz-TDS imaging has no harm to human body, nor can it pollute samples.

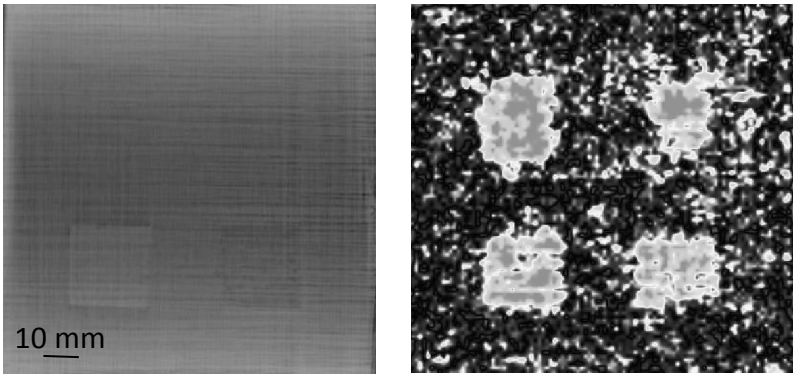

Fig. 7 Detection results of the sample: (a) X-ray CT image slice at depth 1.45 *mm* in the axial direction; (b) reflected ultrasonic image.

4. Summary and conclusion

In this paper, we have inserted different material films into the epoxy GFRP solid panel to simulate the inclusion defects, and we have employed THz-TDS, X-ray CT, and ultrasonic system to detect the defects too. The experimental results show that the defect detection effect is significantly different due to various material inclusions, which depends on the difference between the inclusions and the epoxy GFRP solid panel. By comparing the detection results of THz-TDS, X-ray CT and ultrasonic imaging, THz-TDS imaging can provide higher contrast ratio

than X-ray CT imaging in detecting different material inclusions hidden in the GFRP solid panel, and has much higher lateral resolution than ultrasonic imaging. In addition, THz-TDS technology has no harm to the human body and does not pollute the sample during the detection process. Therefore, THz-TDS technology is hopeful to be an effective alternative to and/or useful complement for the traditional NDE methods.

Acknowledgement

This work was supported by the Ministry of Science and Technology of China (2015CB755401), National Natural Science Foundation of China (61705120), Department of Science & Technology of the Shandong Province (2017GGX10124, 2017GGX10108), Youth Science Funds of Shandong Academy of Sciences (2017QN0015), and Innovation Program of Shandong Academy of Sciences.

References

[1] S. Parvizi, K. W. Garrett and J. E. Bailey. “Constrained cracking in glass fibre-reinforced epoxy cross-ply laminates”. *J. Mater. Sci.*, 13, 195-201 (1978).

[2] I. Amenabar, A. Mendikute, A. López-Arraiza, et.al. “Comparison and analysis of non-destructive testing techniques suitable for delamination inspection in wind turbine blades”. *Compos. Part. B: Eng.*, 42, 1298-1305 (2011).

[3] L. Cheng and G. Y. Tian. “Comparison of nondestructive testing methods on detection of delaminations in composites”. *J. Sensors.*, 3, 276-283 (2012).

[4] J. Tao, L. H. Lee and J. C. Bilello. “Non-destructive evaluation of residual stresses in thin films via x-ray diffraction topography methods”. *J. Electron. Mater.*, 20, 819-825 (1991).

[5] T. E. Michaels and B. D. Davidson. “Ultrasonic inspection detects hidden damage in composites”. *Adv. Mater. Prpcess.*, 143, 34–38 (1993).

[6] A. D. Plessis, S. G. L. Roux and A. Guelpa. “Comparison of medical and industrial x-ray computed tomography for non-destructive testing”. *Nondestruct. Test. Eva*., 6, 17-25 (2016).

[7] A. K. Agrawal, P. S. Sarkar, Y. S. Kashyap, et.al. "Application of x-Ray ct for non-destructive characterization of graphite fuel-yube". *J. Nondestruct. Eval.*, 35, 1-8 (2016).

[8] M. Kersemans, A. Martens, K. V. D. Abeele, et.al. "Detection and localization of delaminations in thin carbon fiber reinforced composites with the ultrasonicpolar scan". *J. Nondestruct. Eval.*, 33, 522-534. (2014).

[9] W. Harizi, S. Chaki, G. Bourse, et.al. "Mechanical damage characterization of glass fiber reinforced polymer laminates by ultrasonic maps". *Compos. Part. B:Eng.*, 70, 131-137 (2015).

[10] F. Ospald, W. Zouaghi, R. Beigang, et.al. "Aeronautics composite material inspection with a terahertz time-domain spectroscopy system". *Opt. Eng.*, 53, 031208 (2014).

[11] C. Stoik, M. Bohn, and J. Blackshire. "Nondestructive evaluation of aircraft composites using reflective terahertz time domain spectros-copy". *NDT&E. Int.*, 43, 106-115 (2010).

[12] F. Rutz, M. Koch, S. Khare, et.al. "Terahertz quality control of polymeric products". *J. Infrared. Milli. Waves.*, 27, 547-556 (2006).

[13] I. Amenabar, F. Lopez and A. Mendikute. "In introductory review to THz non-destructive testing of composite mater". *J. Infrared. Millim. TE.*, 34, 152-169 (2013).

[14] J. Zhang, C. Shi, Y. Ma, et.al. "Spectroscopic study of terahertz reflection and transmission properties of carbon-fiber-reinforced plastic composites". *Opt. Eng.*, 54, 054106 (2015).

[15] J. Zhang, W. Li, H. L. Cui, et.al. "Nondestructive evaluation of carbon fiber reinforced polymer composites using reflective terahertz imaging". *Sensors.*, 16, 875-887 (2016).

[16] K. H. Im, I. Y. Yang, S. K. Kim, et.al. "Terahertz scanning techniques for paint thickness on CFRP composite solid laminates". *J. Mech. Sci. Technol.*, 30, 4413-4416 (2016).

[17] C. Roman, O. Ichim, L. Sarger, et.al. "Terahertz dielectric characterisation of polymethacrylimide rigid foam: the perfect sheer plate". *Electron. Lett.*, 40, 1167-1169 (2004).

[18]. L. Y. Xing, H. L. Cui, C. C. Shi, et.al. "Void and crack detection of polymethacrylimide foams based on terahertz time-domain spectroscopic imaging". *J. Sandw. Struct. Mater.*, 19, 348-363 (2016).

[19]. L. Y. Xing, H. L. Cui, C. C. Shi, et.al. "Nondestructive examination of polymethacrylimide composite structures with terahertz time-domain spectroscopy". *Polym. Test.*, 57, 141-148 (2017).

[20] K. Naito, Y. Kagawa, S. Utsuno, et.al. "Dielectric properties of eight-harness-stain fabric glass fiber reinforced polyimide matrix composite in the THz frequency range". *NDT&E. Int.*, 42, 441-445 (2009).

[21] J. Zhang, J. Wang, X. H. Han, et.al. "Noncontact detection of Teflon inclusions in glass-fiber-reinforced polymer composites using terahertz imaging". *Appl. Opt.*, 55, 10215-10222 (2016).

[22] D. H. Han and L. H. Kang. "Nondestructive evaluation of GFRP composite including multi-delamination using THz spectroscopy and imaging". *Compos. Struct.*,185, 161-175 (2017).